Crystallization of Asymmetric Diblock Copolymers from Microphase-Separated Melts

Daniel J. Quiram and Richard A. Register*

Department of Chemical Engineering, Princeton University, Princeton, New Jersey 08544

Gary R. Marchand

The Dow Chemical Company, P.O. Box 400, Plaquemine, Louisiana 70765

Received October 15, 1996; Revised Manuscript Received May 13, 1997[⊗]

ABSTRACT: Microphase separation in semicrystalline block copolymers can be driven by two forces: thermodynamic incompatibility between the blocks in the melt or crystallization of one or more blocks. The diblock copolymers investigated here are polyethylene-*b*-poly(3-methyl-1-butene), all containing ≈26 wt % ethylene, prepared by hydrogenating high-1,4-polybutadiene-*b*-high-3,4-polyisoprene. This block asymmetry leads to a hexagonally-packed cylindrical morphology when microphase separation is present in the melt. The molecular weights are varied to obtain differing degrees of incompatibility in the melt, ranging from a single-phase (disordered) melt to a strongly segregated melt. X-ray scattering and differential scanning calorimetry are used to investigate the morphology resulting from crystallization in these melts as a function of thermal history. Crystallization from strongly segregated melts is confined to the cylindrical microdomains and produces a morphology essentially independent of thermal history. In the most strongly segregated diblock crystallized at 10−20 °C/min, chain folding within these cylindrical microdomains is preferentially oriented with the chain axis tilted 18 ± 4° from normal to the cylinder axis. In contrast to strongly segregated melts, the morphology produced by crystallization from weakly segregated melts is highly dependent upon thermal history. Faster cooling kinetically confines crystallization to cylinders, while slower cooling results in complete disruption of the cylindrical melt mesophase upon crystallization, leading to a lamellar morphology with a larger domain spacing.

I. Introduction

Microphase separation in semicrystalline block copolymers can be driven either by block incompatibility or by crystallization of one or more blocks. Prior work[1] on the ethylene-*b*-(ethylene-*alt*-propylene) system (E/EP) has demonstrated that when the block incompatibility is small, crystallization proceeds from a single-phase melt and alternating lamellar microdomains result regardless of the copolymer composition (weight fraction of ethylene block, f_E, ranging from 0.12 to 0.56), as anticipated in theoretical treatments.[2,3] Two recent studies employing time-resolved simultaneous small- and wide-angle X-ray scattering (SAXS and WAXS) were performed on diblock copolymers containing an ethylene (E) block which crystallized from a homogeneous melt.[4,5] Both groups concluded that E block crystallization and microdomain formation follow the same growth kinetics. In this study, we examine the control of crystallization through the formation of a melt mesophase.

The establishment of an ordered melt morphology is an added complexity for semicrystalline block copolymers. With an increase in the block incompatibility, microphase separation may occur in the melt prior to crystallization. The presence of melt microdomains affects the crystallization process and the resultant morphology, as previously investigated by a number of groups.[5−14] Time-resolved scattering experiments have been performed on many diblock copolymers containing an ethylene (E) block, during crystallization from microphase-separated melts.[5,6] Rangarajan *et al.*[6] examined the crystallization of an ethylene-*b*-(head-to-head propylene) copolymer (E/hhP) from a weakly segregated lamellar melt (order−disorder transition temperature $T_{ODT} \approx 125$ °C) and found that crystallization induced simultaneous rearrangement of the microdomain structure. The final morphology of the E/hhP diblock was found to be path-dependent (sensitive to minor changes in thermal history) due to melt segregation, which presented a substantial barrier to this microdomain reorganization. Ryan *et al.*[5] examined the crystallization of a series of ethylene-*b*-ethylethylene (E/EE) copolymers ($f_E = 0.25$, 0.49, and 0.75) from microphase-separated melts ($T_{ODT} \approx 255$, 121, and 148 °C, respectively). They found that crystallization destroyed the microphase-separated melt morphologies for all compositions. Of particular relevance to the present work is the sample with $f_E = 0.25$, which in the melt formed a morphology of E cylinders packed onto a hexagonal lattice in an EE matrix. Upon crystallization, the cylindrical melt morphology was transformed into a lamellar structure. Thus, for moderate degrees of melt segregation, crystallization disrupts the melt mesophase to form a lamellar crystalline morphology.

Although modest degrees of segregation are ineffective at confining crystallization, several groups[7−12] have been able to isolate crystallization to microdomains, or to the matrix of a structure containing unperturbed microdomains, through vitrification of one of the blocks. Cohen *et al.*[7] explored the crystallization of an ethylene-*b*-styrene diblock ($f_E = 0.11$) and concluded that crystallization could be confined to spherical microdomains of the polyethylene block when preceded by microphase separation. In this case, the polystyrene matrix ($T_g \approx 100$ °C) is glassy at the freezing point of the polyethylene blocks. Other groups[8−10] have been able to preserve the melt microstructure on crystallization by rapid quenching. Khandpur *et al.*[8] examined morphologies of several polyethylene-containing diblock copolymers after crystallization, through transmission electron microscopy (TEM) on stained samples. One particular E/EP ($f_E = 0.65$) formed EP cylinders in an E matrix in the melt.

* To whom correspondence should be addressed.

[⊗] Abstract published in *Advance ACS Abstracts,* July 15, 1997.

S0024-9297(96)01524-0 CCC: $14.00

Table 1. E/MB Molecular Characterization Data

			I				E			MB
								T_c (°C)		
sample	M_w (kg/mol)	f_E	3,4 addn	1,4 addn	1,2 addn	T_{ODT} (°C)	T_m (°C)	10 °C/min	20 °C/min	T_g (°C)
E/MB35	34.7	0.26	0.58	0.30	0.12	<106	107	80	76	−6
E/MB44	44.3	0.26	0.54	0.36	0.10	167	105	71	64	−10
E/MB63	62.7	0.27	0.50	0.42	0.080	>260	105	62	61	−17
E/MB88	87.9	0.27	0.47	0.47	0.058	>260	103	62	61	−20

While the microstructure was distorted beyond recognition when the sample was cooled at a moderate rate (in an ice water bath), the cylindrical melt morphology was preserved if the sample was quenched in liquid nitrogen. A similar approach had been employed previously by Sakurai *et al.*[9] to "freeze" the melt microstructure of a polyethylene-containing diblock blended with an amorphous homopolymer. Tepe and co-workers[10] investigated an E/EP diblock copolymer forming E cylinders in the melt ($f_E = 0.37$, $T_{ODT} = 189$ °C), the inverse of the material studied by Khandpur *et al.*,[8] and demonstrated via small-angle neutron scattering (SANS) that quenching in liquid nitrogen led to crystallization within the cylindrical microdomains. While these studies have been successful in confining crystallization to preexisting microdomains, relying on vitrification of one component limits the generality of this approach. The use of a polymer with a glassy matrix obviously restricts the possible range of physical properties (and, in particular, precludes the use of materials suitable as thermoplastic elastomers), while quenching in liquid nitrogen is not a practical thermal processing technique.

Rather than relying on vitrification of one block, here we explore whether increased interblock segregation strength can effectively constrain crystallization to predefined regions of the melt mesophase, such as cylinders or spheres, under conventional crystallization conditions. Although crystallization in weakly segregated melts and vitrified systems has been studied extensively, crystallization from strongly segregated melts has not been investigated, nor has there been a systematic study of the effect of segregation strength on the solid-state morphology. Our system consists of a series of ethylene-*b*-3-methyl-1-butene (E/MB) diblock copolymers of constant composition ($f_E \approx 0.26$) and varying molecular weight. The T_g of both blocks is below room temperature, so the final morphology will not be controlled by vitrification under conventional cooling conditions. The effect of thermal history on the crystallization from melts ranging from single phase to strongly segregated is closely examined.

II. Experimental Section

A. Synthesis and Molecular Characterization. The E/MB precursors, (high-1,4-butadiene)-*b*-(high-3,4-isoprene), were synthesized via sequential anionic polymerization in cyclohexane. To create the high-3,4-isoprene precursor to the MB block, 1,2-dipiperidinoethane (DPE) was added at a concentration of 2 mol/(mol of Li initiator) after polymerization of the 1,4-butadiene block.[15] The E/MB diblocks were prepared from the precursors by exhaustive hydrogenation at 100 °C and 400 psi in heptane using unreduced palladium on barium sulfate as catalyst.[16] Fourier transform infrared spectroscopy (FTIR) was used to verify that there was no residual unsaturation in the samples. ^{1}H nuclear magnetic resonance (NMR) of the precursors resulted in considerable overlap of the olefinic resonances due to the various types of addition present in both blocks. Due to the complicated ^{1}H NMR spectra of these polymers, selective hydrosilation[17] and other techniques were used to determine the block composition and microstructure of the precursors.[18] The 1,2 content in the butadiene block was presumed to be 8.5% for all polymers on the basis of polymerization conditions and the melting temperatures of the E blocks.

Molecular weights and polydispersities of the precursor diblocks were determined by low-angle laser light scattering (LALLS; Chromatix KMX-6) in cyclohexane and by gel permeation chromatography (GPC) in tetrahydrofuran. A refractive index increment (dn/dc) value of 0.108 mL/g was used for 1,4-polybutadiene (8.5 wt % 1,2 addition) in cyclohexane.[19] The refractive index increments of polyisoprenes (50 and 93% 1,4 addition) in cyclohexane are very similar to those for polybutadienes when compared at the same 1,4 content.[19] Since dn/dc values for polybutadienes of various microstructures in cyclohexane are well-known[19,20] and less information is available for polyisoprenes, we used polybutadiene values (matching the 1,4 content) to represent our high-3,4-isoprene block. Using this method, the weight-averaged dn/dc values for the four samples varied from 0.097 to 0.100 mL/g (from E/MB35 to E/MB88). High-temperature GPC of the E/MB diblocks at 135 °C in 1,2,4-trichlorobenzene showed that no backbone rearrangements occurred as a result of hydrogenation.

The molecular characterization results are listed in Table 1. Note that the 3,4 content of the isoprene block decreases with increasing molecular weight. During synthesis, a fixed DPE:Li ratio and monomer concentration were used; therefore, the concentration of DPE is lower for higher molecular weight materials. Less than 10% 1,4 addition can be achieved using a 5:1 DPE:Li ratio at room temperature.[15] This variability of the isoprene microstructure influences the interactions between E and MB units in the hydrogenated polymers, and thus the Flory interaction parameter χ is slightly different for each polymer. However, since we directly measure (or bound) T_{ODT} for each sample, this is not a significant complication.

B. Thermal and Morphological Characterization. Flow-induced alignment of cylinders in block copolymers was first demonstrated by Keller *et al.*[21] Here, orientation was achieved using a lubricated channel die based on the design of Khan and Larson.[22] Molding[23] was performed at 150 °C, using compression ratios of 5.8 (E/MB44), 7.2 (E/MB63), and 11 (E/MB88) and holding the processed strip in the die at 150 °C for 15 min before cooling at 10−20 °C/min by running water through the press platens.

A Perkin-Elmer DSC-7 was used to measure thermal transitions and isothermal crystallization rates of the E/MB samples. Differential scanning calorimetry (DSC) calibration was performed using indium and mercury or zinc standards. A heating rate of 10 °C/min and cooling rates of 10 and 20 °C/min were used to determine the final melting temperature (T_m of E block), the enthalpy of melting (ΔH_m of E block), the peak crystallization temperature (T_c of E block), and the glass transition temperature (T_g of MB block). Isothermal DSC runs were started at 150 °C followed by a fast quench (≈250 °C/min) to the crystallization temperature.

One-dimensional SAXS data were collected using an Anton-Paar compact Kratky camera connected to a position sensitive detector (Braun OED-50M). The data were reduced using previously reported procedures[24] to desmeared absolute intensity versus the scattering vector $q = (4\pi/\lambda) \sin \theta$, where λ is the radiation wavelength and 2θ is the scattering angle. Static SAXS data were acquired at different temperatures through the use of a hot stage.[25] Two thermal histories were used to crystallize these samples. The first, referred to as *fast cooled*, involved heating samples to 140 °C in a PHI platen press under pressures not exceeding 125 psi, holding them at temperature for 5 min, and cooling them to room temperature

at 10−20 °C/min. Samples labeled as *slow cooled* were heated to 150 °C in the SAXS hot stage, held at temperature for at least 15 min, cooled at ≈8 °C/min to the crystallization temperature, held at this temperature for at least four times the crystallization half-time ($t_{1/2}$, as determined by isothermal DSC), and finally cooled at ≈4−5 °C/min to room temperature. For a lamellar microstructure, d is the sum of the E and MB domain widths and is determined from the position of the first peak q^* in the q^2-corrected[26] data:

$$d = 2\pi/q^* \quad (1)$$

For a two-dimensional hexagonally-packed cylindrical microstructure, d corresponds to the (10) planes and is similarly determined from q^* in the q-corrected[26] data. In addition, a relative measure of the breadth of the interdomain distance distribution may be obtained from the breadth of the first-order reflection Δq, which is determined as the peak width at 85% of the maximum intensity.

SAXS with an area detector and point collimation was performed on the oriented samples. In this case, X-rays were generated from a Rigaku RU-200BH rotating anode generator equipped with a 0.2 × 0.2 mm microfocus cathode and Franks mirror optics. Samples were placed inside an evacuated sample chamber. Two dimensional diffraction images were collected with an image-intensified area detector designed around a Thomson CCD chip.[27] After collection, images were digitized and corrected for detector response characteristics. WAXS was performed on the oriented E/MB88 sample employing a Philips XRG-3000 sealed tube generator, Huber 151 graphite monochromator, a Statton pinhole camera (W. H. Warhus), and Kodak image plates read with a Molecular Dynamics Phosphorimager SI scanner. In all three X-ray apparatuses, Cu Kα radiation was selected.

Small-angle light scattering (SALS) H_v patterns[28] were obtained with a helium−neon laser, screen, and NEC TI-22A CCD camera.[29] Samples with varying thermal histories were crystallized for SALS using a Mettler FP82 hot stage.

III. Results and Discussion

A. Microdomain Morphology following Crystallization from Strongly Segregated Melts. We consider the two highest molecular weight samples, E/MB63 and E/MB88, as having strongly segregated melts. The ODT temperatures of both samples exceeded the 260 °C upper use temperature of the SAXS hot stage. Figures 1 and 2 illustrate the effect of thermal history on the morphology of E/MB63 and E/MB88. The bottom profile in these figures was taken in the melt at 110 °C and shows an intense, narrow primary peak and, for E/MB63, a shoulder at $\sqrt{3}q^*$ along with a peak at $\sqrt{7}q^*$, indicating a hexagonally-packed cylindrical microstructure, as expected for block copolymers with $f = 0.27$. The upper three SAXS profiles are from crystallized samples at room temperature with differing thermal histories. The final crystalline morphology of these samples is largely independent of thermal history, as indicated by the nearly constant position of the primary peak. A small q^* decrease is observed for the crystalline samples in comparison with the melt at 110 °C, which will be discussed in section C; however, the very limited q^* change observed in Figures 1 and 2 suggests that crystallization is being confined to the cylindrical microdomains in these two samples, independent of thermal history.

To reinforce this conclusion, a sample of E/MB88 was flow-aligned in a lubricated channel die in the melt at 150 °C. The expected alignment of cylinders as taken from ref 23 is shown in the inset in Figure 3, with the cylinder axes along the flow direction. Following alignment, the sample was cooled in the channel die down to room temperature at a rate of 10−20 °C/min, crystallizing during the process. Slices of this aligned, crystallized sample were investigated at room temperature with 2D SAXS. Figure 3 shows the image taken with the X-ray beam along the flow direction. Five spots are evident at $q^* = 0.130$ nm^{-1} with an azimuthal peak-to-valley ratio of over 14 (a sixth reflection is blocked by the beam stop). This persistence of 6-fold symmetry following crystallization proves that the polyethylene blocks are indeed crystallizing within the preestablished cylindrical microdomains. To our knowledge, this is the

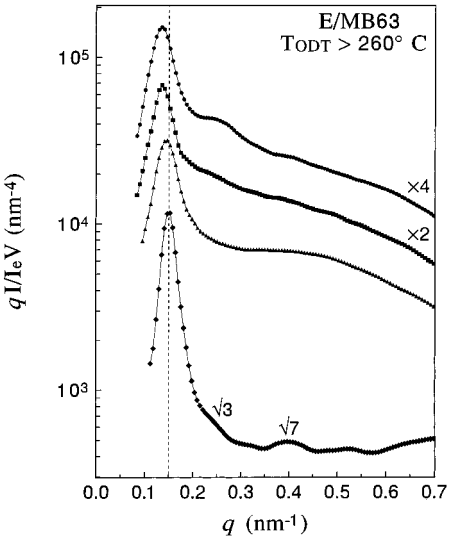

Figure 1. SAXS profiles (q-corrected) for E/MB63 as a function of thermal history. The bottom profile (♦) was taken in the melt at 110 °C, while the upper three profiles were taken on crystalline samples at room temperature with differing processing histories: fast cooled (▲), slow cooled to 65 °C (■), and slow cooled to 85 °C (●). The upper two profiles have been shifted along the intensity axis as indicated for clarity. Note that the primary peak position of the crystalline samples is quite similar to that of the melt and is largely independent of thermal history.

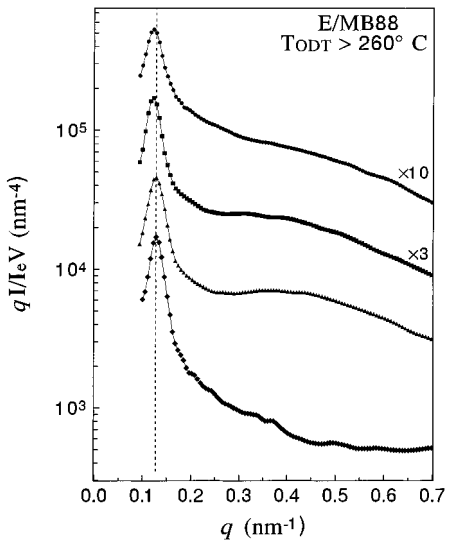

Figure 2. SAXS profiles (q-corrected) for E/MB88 as a function of thermal history. The bottom profile (♦) was taken in the melt at 110 °C, while the upper three profiles were taken on crystalline samples at room temperature with differing processing histories: fast cooled (▲), slow cooled to 65 °C (■), and slow cooled to 80 °C (●). The upper two profiles have been shifted along the intensity axis as indicated for clarity. Note that the primary peak position of the crystalline samples is quite similar to that of the melt and is largely independent of thermal history.

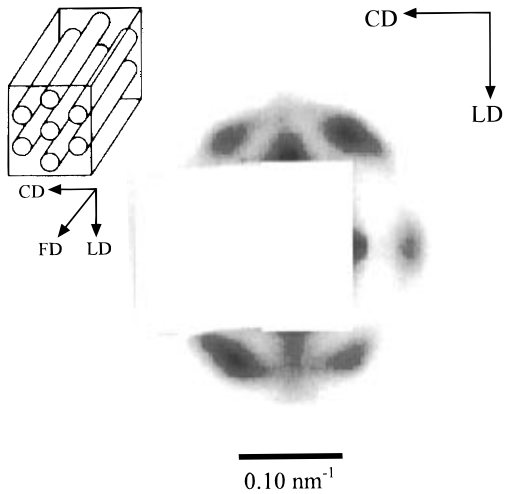

Figure 3. 2D SAXS image taken on an oriented, crystallized sample of fast cooled E/MB88 at room temperature with the X-ray beam along the channel die flow direction (FD, cylinder axis). The inset shows the orientation of the cylinders and the loading (LD) and constraint (CD) directions in the channel die. Five spots of the primary reflection are evident, with a sixth positioned behind the beam stop.

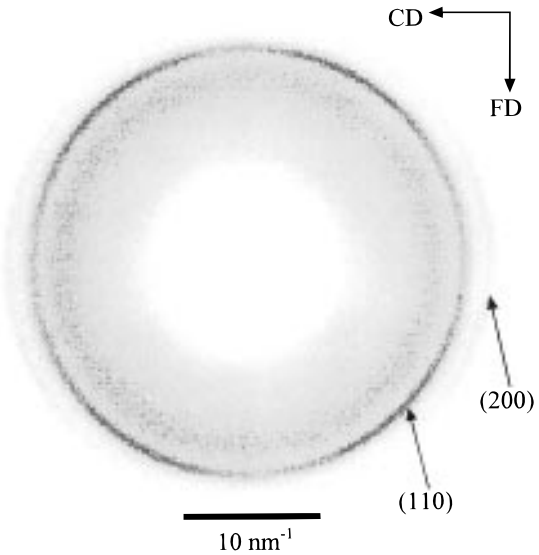

Figure 4. Two dimensional WAXS image taken on an oriented sample of fast cooled E/MB88 at room temperature with the X-ray beam along the channel die loading direction. On the basis of the SAXS pattern of Figure 3, the cylinder axis is vertical in the present figure, and the constraint (CD) and flow (FD) directions in the channel die are indicated. The diffuse inner ring is the unoriented amorphous halo. The first crystalline reflection is due to the (110) planes of orthorhombic polyethylene and displays four regions of high intensity. A second crystalline reflection, (200), is preferentially located on the equator.

first experimental evidence of crystallization effectively templated by the mesophase structure of a polymer, even though both blocks are fluid at the crystallization conditions and crystallization occurs at typical or even slow rates (*e.g.*, no quenching in liquid nitrogen). Similar results via 2D SAXS have also been obtained for E/MB88 slow cooled to 71 °C ($t_{1/2} \approx 5$ min) and E/MB63 both fast cooled and slow cooled to 77 °C ($t_{1/2} \approx 5$ min).[18]

B. Crystallite Orientation following Crystallization from Strongly Segregated Melts. The direction of chain folding in semicrystalline block copolymers is a topic of interest which has been investigated by several groups.[1,6,30−33] Rangarajan *et al.*[1,6] inferred E chain folding with the chain axis normal to the lamellar interface for E/EP diblock copolymers crystallizing from homogeneous melts, based on the presence of spherulites in the solid state. Yang and coworkers[30] observed this same direction of chain folding based on SAXS and Raman spectroscopy measurements for low-molecular weight block copolymers containing ethylene oxide which crystallized from single-phase or weakly segregated melts. Conversely, Douzinas and Cohen[31] found that the E chain axis runs parallel to the domain interface in E/EE diblocks which crystallize from a heterogeneous melt through pole figure analysis on aligned samples. More recently, Hamley *et al.*[32,33] observed this same chain orientation in E/EE diblocks and a symmetric ethylene-*b*-vinylcyclohexane diblock (semicrystalline-glassy) through 2D WAXS on shear oriented samples. Thus, in lamellar systems, chain folding appears to vary depending on the state of the material (homogeneous, microphase-separated, partially vitrified) at the crystallization conditions.

To investigate the direction of chain folding within cylindrical microdomains, 2D WAXS images were taken on the oriented fast cooled E/MB88 sample at room temperature. Figure 4 shows the image obtained with the beam along the loading direction with three rings evident: the unoriented, broad inner ring is due to scattering from amorphous segments, while the outer two oriented rings correspond to the (110) and (200) reflections of the orthorhombic E unit cell. Both of the

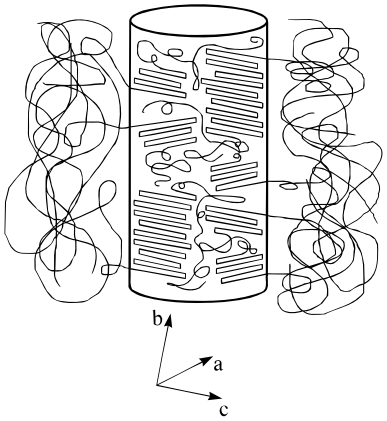

Figure 5. Schematic of the orientation of chain folding when crystallization is confined to cylindrical microdomains. In fast-cooled E/MB88, the chain axis preferentially aligns 18 ± 4° from normal to the cylinder axis. The $a-c$ directions of the polyethylene unit cell are as indicated; the b axis is tilted 18° from the cylinder axis.

crystalline reflections are preferentially oriented, with the (110) reflection displaying four off-axis azimuthal maxima and the (200) reflection exhibiting two arcs with maximum intensity on the equator. Averaging data from four images taken from different spots on the oriented sample, the (110) peaks are separated by an angle of 54 ± 1.5° from the horizontal axis. The analogous image with the beam along the constraint direction is similar to Figure 4, while the image taken with the beam along the flow direction shows unoriented (110) and (200) rings. On the basis of the separation angle between regions of high intensity in the (110) reflection and unit cell dimensions taken from ref 34, the chain axis is preferentially tilted at an angle of 18 ± 4° from the cylinder axis normal as shown in Figure 5 (chains perpendicular to the interface would result in (110)

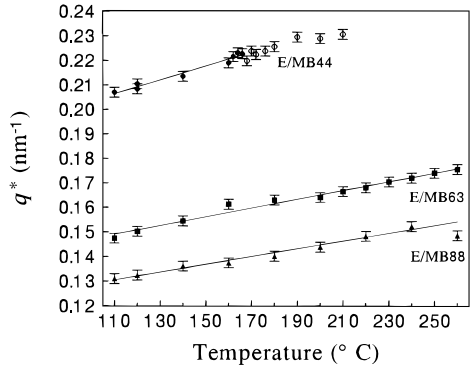

Figure 6. Primary peak position (q^*) as a function of temperature in the melt for E/MB44 (●,○), E/MB63 (■), and E/MB88 (▲). Note that q^* increases with temperature for all three materials shown. E/MB63 and E/MB88 remain microphase-separated up to at least 260 °C, while T_{ODT} for E/MB44 is 167 °C. For E/MB44, closed symbols (●) correspond to microphase-separated melts, while open symbols (○) were taken from correlation hole peaks[37] in homogeneous melts. Linear fits of the microphase-separated data are shown by the lines.

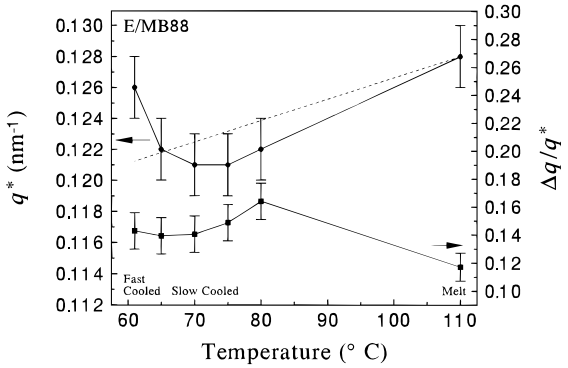

Figure 7. Primary peak position (q^*, ●) and breadth ($\Delta q/q^*$, ■) for E/MB88 as a function of crystallization temperature (melt data shown at 110 °C, fast cooled data at 61 °C). See Figure 2 for SAXS profiles. The dashed line is an extrapolation of the fit of the melt q^* data shown in Figure 6. Note that the same slope is used as in Figure 6, but the line is shifted down to adjust for a slightly different value of q^* (experimental uncertainty, 2%, as indicated by error bars) at 110 °C.

peaks separated by an angle of 58° from the horizontal). Tilt angles ranging from 18 to 45° with respect to the lamellar interface normal have previously been observed in the crystallization of low-molecular weight linear polyethylene homopolymers.[35,36] If the chain axis were aligned parallel to the cylinder axis, a standard fiber pattern would result with all (hk0) reflections situated on the equator. The type of chain folding observed within these cylinders is different than the chain folding which has been observed in crystallization from segregated lamellar melts, where the chain axis lies parallel to the microdomain interfaces.[31−33] Further 2D SAXS and WAXS studies involving oriented E/MB samples are currently in progress.

C. Microdomain Spacing following Crystallization from Strongly Segregated Melts. Returning to the small differences in q^* between melt and solid which are evident in Figures 1 and 2, we first examine the temperature dependences of the primary peak positions in the melt. The melt q^* of both E/MB63 and E/MB88 increases linearly with temperature (see Figure 6; E/MB44 data also included). Over a 130 °C range (110 to 240 °C), q^* increases 17% for E/MB63 and 16% for E/MB88. Such a strong temperature dependence of q^* is not unprecedented, as Sakamoto and Hashimoto[38] observed a 10% increase in q^* over a range of 100 °C in a styrene-*b*-isoprene copolymer. A number of effects may contribute to this q^* trend, including bulk thermal expansion and changes in both the statistical segment length and the block incompatibility with temperature. The strong segregation model of Helfand and Wasserman[39−41] incorporates these effects and was used for domain spacing calculation. Neglecting the microstructure variation in the MB block, we can bound $\chi(T)$ for E/MB based on the known T_{ODT} for E/MB44 (see section D) and the lower bound on T_{ODT} for E/MB63 (>260 °C). Temperature-dependent densities and statistical segment lengths were taken from refs 19 and 42. With the steepest $\chi(T)$, 14% increases in q^* are predicted over the 110−240 °C range. In addition, the absolute values of q^* predicted by the model are within 1 (E/MB44), 9 (E/MB63), and 5% (E/MB88) of the experimental values over the same temperature range.

Using the data in Figure 6, linear fits of q^* as functions of temperature can be made for E/MB63 and E/MB88 and extrapolated down to the crystallization temperatures used (see dashed line in Figure 7 for E/MB88). Both fits predict a 5% decrease in q^* between the melt (110 °C) and the crystallized samples (slow cooled to T_c of 65−70 °C) versus the observed values of 8 (E/MB63) and 5% (E/MB88). From the fit extrapolation in Figure 7, it can be seen that the peak positions for all crystallized samples are within experimental uncertainty of the extrapolation from the melt, with the exception of the fast cooled sample. Therefore, the observed decrease in q^* for E/MB63 and E/MB88 upon crystallization in the slow cooled specimens results from an increase in the interdomain spacing of the microphase-separated melt prior to the onset of crystallization. This will be discussed more fully in an upcoming paper on the kinetics of structure development in the E/MB system.[43] There is little change in q^* when these materials are fast cooled because crystallization proceeds quickly and there is insufficient time for chain diffusion to significantly adjust the interdomain distance in the melt prior to crystallization; thus, the fast cooled q^* is significantly larger than the extrapolated value as seen in Figure 7.

The peak breadth $\Delta q/q^*$ for E/MB88 is also plotted in Figure 7. This shows a modest increase between the melt at 110 °C and the crystallized samples, since crystallization causes some distortion of the melt mesophase structure. Note that $\Delta q/q^*$ is largest for the sample which crystallized the most slowly (slow cooled to 80 °C, $t_{1/2}$ = 22 min), with subsequent values decreasing as the speed of crystallization increases. This result indicates that the more quickly crystallization is forced to occur, the better the melt microstructure is preserved, as already evidenced by the extreme case of quenching in liquid nitrogen.[8]

The development of spherulites by a semicrystalline polymer implies the existence of lamellae, since spherulites are known to grow as lamellar crystals radiating from a central nucleus.[44] If crystallization is confined to cylindrical microdomains, crystal growth cannot lead to larger-scale arrangement into spherulites. As expected, E/MB63 and E/MB88 samples crystallized in manners similar to those described in Figures 1 and 2 did not show the cloverleaf pattern in H_v SALS, even for the most slowly crystallized samples.

D. Crystallization from a Weakly Segregated Melt. A lower molecular weight sample, E/MB44, was

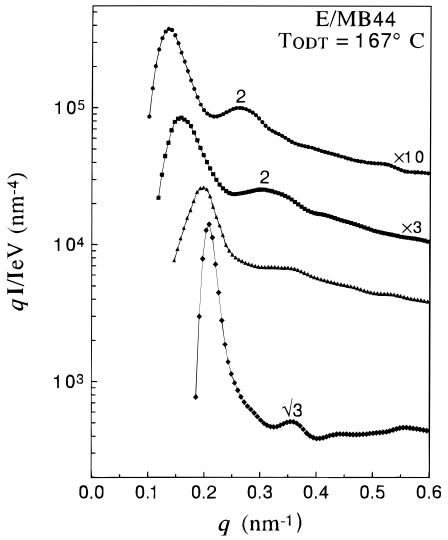

Figure 8. SAXS profiles (q-corrected) for E/MB44 as a function of thermal history. The bottom profile (♦) was taken in the melt at 110 °C, while the upper three profiles were taken on crystalline samples at room temperature with differing processing histories: fast cooled (▲), slow cooled to 70 °C (■), and slow cooled to 90 °C (●). The upper two profiles have been shifted along the intensity axis as indicated for clarity. Note that q^* of the melt is similar to that of the fast cooled sample, while q^* for the slow cooled samples decreases and a second-order peak is evident (both profiles) in a q ratio of 1:2.

found to have an ODT temperature of 167 °C, as determined by SAXS using the method of ref 25. E/MB44 thus has a weakly segregated melt at the crystallization temperature. Figure 8 illustrates the effect of thermal history on the morphology of E/MB44. The bottom profile was acquired in the melt at 110 °C and reflects the expected cylindrical morphology, while the upper three SAXS profiles were collected at room temperature on samples with differing crystallization histories. When E/MB44 is fast cooled from the melt, a small decrease in q^* occurs (0.206 nm^{-1} for the melt at 110 °C vs 0.195 nm^{-1} for the fast cooled sample at room temperature). This 5% decrease in q^* is predicted from an extrapolation of the fit shown in Figure 6. As with E/MB88, E/MB44 was also flow-aligned in a lubricated channel die at 150 °C and then fast cooled. From a 2D SAXS image with the beam along FD (data not shown),[18] hexagonal symmetry was observed, verifying that crystallization was confined to cylinders, although the six spots were rotated 30° relative to the image shown in Figure 3 ((10) cylinder plane normals parallel to LD for E/MB44 vs (11) cylinder plane normals for E/MB88). Both types of orientation have been observed previously in samples oriented via large-amplitude oscillatory shear.[10]

The upper two profiles in Figure 8 resulted from slow cooling to 70 °C ($t_{1/2} \approx 1$ min) and 90 °C ($t_{1/2} \approx 16$ min), respectively. In both cases, there is a significant decrease in q^* along with the emergence of a second-order peak in a q ratio of 1:2, reflecting a lamellar morphology. Thus, slow crystallization breaks out of the cylindrical melt microstructure and forms alternating E and MB lamellae. Further evidence of this transformation comes from H_v SALS: E/MB44 slow cooled to between 70 and 90 °C exhibits spherulite formation, while fast cooled E/MB44 does not. The lamellar repeat distance decreases from 46.2 nm at T_c = 90 °C to 40.0 nm at 70 °C, indicating that faster crystallization (at 70 °C) limits the magnitude of the

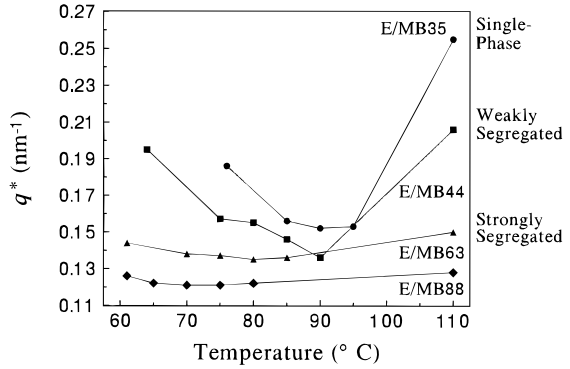

Figure 9. Primary peak position (q^*) as a function of crystallization temperature (melt data shown at 110 °C, fast cooled data at T_c, 20 °C/min (see Table 1)) for E/MB35 (●), E/MB44 (■), E/MB63 (▲), and E/MB88 (♦). See Figures 1, 2, and 8 for SAXS profiles.

domain spacing change; similar results were previously observed by Rangarajan *et al.* for a lamellar E/hhP diblock.[6] Since slow crystallization leads to lamellae, the cylindrically confined crystallization observed for fast cooling in E/MB44 is a kinetic phenomenon.

E. Crystallization from a Single-Phase Melt. The lowest molecular weight sample, E/MB35, forms a homogeneous melt. Regardless of thermal history, two SAXS peaks are evident for crystalline samples. These peaks are in a q ratio of 1:2, indicating that a lamellar microstructure is formed, as expected.[1] Unlike the E/EP diblocks studied previously,[1] thermal history has an effect on lamellar spacing for E/MB35. This distinction between E/MB35 and the E/EP series is most likely due to the fact that E/MB35 is "nearly segregated" in the melt; from 120 to 106 °C, the correlation hole peak observed by SAXS more than doubles in intensity, suggesting an ODT only moderately below the melting point. Composition fluctuations close to the ODT evidently slow chain diffusion and create a thermal history dependence of the crystalline morphology. H_v SALS results showed the cloverleaf pattern for all E/MB35 samples, regardless of crystallization conditions (fast and slow cooled).

A summary of the primary SAXS peak position results for all four samples is given in Figure 9, where q^* is plotted versus temperature (melt, 110 °C)/crystallization temperature (all others). The two diblocks which showed strongly segregated melts, E/MB63 and E/MB88, display a small range of q^* values over the various crystallization conditions. In contrast, the sample with the weakly segregated melt (E/MB44) shows a strong dependence of q^* on thermal history, with the fast cooled (T_c = 64 °C) and melt values being quite similar. Lastly, E/MB35, which crystallized from a homogeneous melt, also exhibits a q^* difference between the fast cooled and slow cooled runs, as well as between the fast cooled specimen and the disordered melt.

F. Crystallinities Obtained under Different Crystallization Conditions. While Figure 9 addresses the size scale of the microdomain structures, it says nothing about the level of crystallinity. It seems plausible that the weight fraction crystallinity (w_c) would decrease when crystallization is confined to cylinders, due to the difficulty of packing crystalline units into a domain with curved interfaces. To explore this point, the thermal conditions used for SAXS as described in the Experimental Section were duplicated with the DSC-7. Following cooling of the samples to room temperature, a heating run was performed from

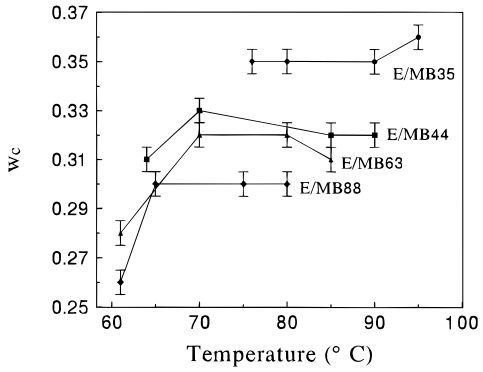

Figure 10. Weight fraction crystallinity (w_c) as determined by eq 2 as a function of crystallization temperature for E/MB35 (●), E/MB44 (■), E/MB63 (▲), and E/MB88 (♦). The leftmost data point for each material corresponds to a fast cooled specimen and is plotted at the T_c value (exotherm peak) on cooling at 20 °C/min.

0 to 150 °C at a scan rate of 10 °C/min. Then, w_c of the E block for each of the DSC runs was calculated using

$$w_c = \frac{\Delta H_m}{(\Delta H_m)_{100\%} f_E} \tag{2}$$

In eq 2, $(\Delta H)_{100\%}$ is the theoretical value for 100% crystalline PE which is taken as 277 J/g.[45] The weight fraction crystallinity is plotted vs the crystallization temperature (using T_c at 20 °C/min for the fast cooled samples) in Figure 10. The higher the molecular weight of the E/MB, the lower the weight fraction crystallinity at a given crystallization temperature. E/MB35 has a truly crystallization-driven morphology since it starts as a single-phase melt. With no hindrances to crystallization, this sample consistently contains the most crystallinity along with the highest melting crystals (see Table 1). As the melt becomes more strongly segregated prior to crystallization, the polymers are limited to lower levels of crystallinity and lower-melting crystals in the E block.

It is important to note that the ethyl branches (22/1000 carbons) present in the E block greatly reduce the value of w_c over that expected for a high-density polyethylene block and limit the crystal thickness as well. Consequently, in our E/MB diblocks, it is possible to accommodate the crystals within the E cylinders with only a modest enthalpic penalty (reduced w_c). In these diblocks, the minimum-free-energy state which dictates equilibrium solid-state morphology is governed by a balance between entropy and enthalpy. As with amorphous block copolymers,[39−41] an important contributor to the entropy is chain stretching; as is clear from both Figure 8 and our previous work,[46] the domain spacing tends to increase on crystallization, leading to increased chain stretching in the amorphous block. Unlike amorphous block copolymers, the primary contributor to the enthalpy in our case is crystallization of the E block. If transforming to a lamellar structure with a larger periodicity can produce a higher degree of crystallinity, then this transformation may be favored—particularly as temperature is reduced away from the melting point, where the free energy of crystallization is zero—even though there may be a substantial free energy penalty incurred from the additional chain stretching. For polymers containing blocks which tend to higher levels of crystallinity, such as high-density polyethylene, the increased difficulty in achieving a comparable value of w_c by crystallizing within microdomains should disfavor the type of constrained crystallization we observe here.

The foregoing comments refer to the expected equilibrium morphology in these semicrystalline diblocks, rather than directly bearing on any metastable structures which might form due to kinetic limitations during crystallization. While it is difficult to unambiguously assess whether our samples are at equilibrium or not, the results shown in Figure 8 for E/MB44—where fast crystallization at low temperatures yields cylinders and slow crystallization at higher temperatures yields lamellae—suggests that the cylindrical solid-state morphologies observed for E/MB63 and E/MB88 are metastable as well. Note, however, that these structures are extremely robust: they are reproducibly formed by crystallization even at very slow rates (crystallization half-times greater than 20 min) and are not transformed even by prolonged annealing close to the melting point (8 h anneal at 4 °C below T_m). Therefore, increased melt segregation can effectively constrain crystallization to particular regions of a fully-fluid mesophase, even under conditions where crystallization proceeds slowly.

IV. Conclusions

The morphology in a series of asymmetric (26−27% E) crystallizable E/MB diblock copolymers has been studied as a function of degree of melt segregation under a range of crystallization conditions. The highest molecular weight samples, E/MB63 and E/MB88, form strongly segregated melts (T_{ODT} > 260 °C) with hexagonally-packed E cylinders in an MB matrix. Using both SAXS and H_v SALS, we find that crystallization from these melts is confined to the preestablished cylindrical microdomains for all thermal conditions examined. WAXS measurements on fast cooled E/MB88 indicate that the chains fold within the cylinders such that the chain axis is preferentially tilted at 18 ± 4° from the cylinder axis normal. In contrast to these strongly segregated materials, E/MB44 forms a weakly segregated melt (T_{ODT} = 167 °C), with crystallization resulting in a morphology which is strongly dependent on thermal history. Fast cooling kinetically confines crystallization to cylinders and a spherulitic superstructure is not formed. Slow cooling E/MB44 allows crystallization to break out of the preestablished melt mesophase and form a lamellar morphology exhibiting a larger Bragg spacing than the melt, with the additional development of a spherulitic superstructure. E/MB35, the lowest molecular weight polymer, forms a single-phase melt and crystallizes into a lamellar morphology with a Bragg spacing dependent on thermal history. In summary, sufficiently strong melt segregation can effectively constrain crystallization to parts of the melt mesophase, even when the polymer is fluid and crystallization is slow. However, this templating becomes progressively less effective as the segregation strength is reduced.

Acknowledgment. This work was supported by the National Science Foundation, through the Polymers Program (Grant DMR-9257565). The authors thank the following individuals for their experimental assistance: Dvora Perahia (2D SAXS), Charles Haisch (DSC), David Dean (2D WAXS), and Dee Strand (high-temperature GPC).

References and Notes

(1) Rangarajan, P.; Register, R. A.; Fetters, L. J. *Macromolecules* **1993**, *26*, 4640.

(2) DiMarzio, E. A.; Guttman, C. M.; Hoffman, J. D. *Macromolecules* **1980**, *13*, 1194.
(3) Whitmore, M. D.; Noolandi, J. *Macromolecules* **1988**, *21*, 1482.
(4) Rangarajan, P.; Register, R. A.; Adamson, D. H.; Fetters, L. J.; Bras, W.; Naylor, S.; Ryan, A. J. *Macromolecules* **1995**, *28*, 1422.
(5) Ryan, A. J.; Hamley, I. W.; Bras, W.; Bates, F. S. *Macromolecules* **1995**, *28*, 3860.
(6) Rangarajan, P.; Register, R. A.; Fetters, L. J.; Bras, W.; Naylor, S.; Ryan, A. J. *Macromolecules* **1995**, *28*, 4932.
(7) Cohen, R. E.; Cheng, P. L.; Douzinas, K.; Kofinas, P.; Berney, C. V. *Macromolecules* **1990**, *23*, 324.
(8) Khandpur, A. K.; Macosko, C. W.; Bates, F. S. *J. Polym. Sci., B: Polym. Phys.* **1995**, *33*, 247.
(9) Sakurai, K.; MacKnight, W. J.; Lohse, D. J.; Schulz, D. N.; Sissano, J. A. *Macromolecules* **1993**, *26*, 3236.
(10) Tepe, T.; Schulz, M. F.; Zhao, J.; Tirrell, M.; Bates, F. S.; Mortensen, K.; Almdal, K. *Macromolecules* **1995**, *28*, 3008.
(11) Schnablegger, H.; Rein, D. H.; Rempp, P.; Cohen, R. E. *J. Polym. Eng.* **1996**, *16*, 1.
(12) Robitaille, C.; Prud'homme, J. *Macromolecules* **1983**, *16*, 665.
(13) Nojima, S.; Kato, K.; Yamamoto, S.; Ashida, T. *Macromolecules* **1992**, *25*, 2237.
(14) Séguéla, R.; Prud'homme, J. *Polymer* **1989**, *30*, 1446.
(15) Mays, J.; Hadjichristidis, N.; Fetters, L. J. *Macromolecules* **1984**, *17*, 2723.
(16) Rosedale, J. H.; Bates, F. S. *J. Am. Chem. Soc.* **1988**, *110*, 3542.
(17) Meyers, K. O.; Bye, M. L.; Merrill, E. W. *Macromolecules* **1980**, *13*, 1045.
(18) Quiram, D. J. Ph.D. Thesis, Princeton University, 1997.
(19) Krishnamoorti, R. Ph.D. Thesis, Princeton University, 1994.
(20) Balsara, N. P.; Fetters, L. J.; Hadjichristidis, N.; Lohse, D. J.; Han, C. C.; Graessley, W. W.; Krishnamoorti, R. *Macromolecules* **1992**, *25*, 6137.
(21) Keller, A.; Pedemonte, E.; Willmouth, F. M. *Nature* **1970**, *225*, 538.
(22) Khan, S. A.; Larson, R. G. *Rheol. Acta* **1991**, *30*, 1.
(23) Lee, H. H.; Register, R. A.; Hajduk, D. A.; Gruner, S. M. *Polym. Eng. Sci.* **1996**, *36*, 1414.
(24) Register, R. A.; Bell, T. R. *J. Polym. Sci., B: Polym. Phys.* **1992**, *30*, 569.
(25) Adams, J. L.; Quiram, D. J.; Graessley, W. W.; Register, R. A.; Marchand, G. R. *Macromolecules* **1996**, *29*, 2929.
(26) Russell, T. P. In *Handbook on Synchrotron Radiation*; Brown, G. S., Moncton, D. E., Eds.; North-Holland: New York, 1991; Vol. 3.
(27) Tate, M. W.; Gruner, S. M.; Eikenberry, E. F. *Rev. Sci. Instrum.* **1997**, *68*, 47.
(28) Stein, R. S. *Rubber Chem. Technol.* **1976**, *49*, 458.
(29) Ueda, M. M.S.E. Thesis, Princeton University, 1995.
(30) Yang, Y.-W.; Tanodekaew, S.; Mai, S.-M.; Booth, C.; Ryan, A. J.; Bras, W.; Viras, K. *Macromolecules* **1995**, *28*, 6029.
(31) Douzinas, K. C.; Cohen, R. E. *Macromolecules* **1992**, *25*, 5030.
(32) Hamley, I. W.; Fairclough, J. P. A.; Terrill, N. J.; Ryan, A. J.; Lipic, P. M.; Bates, F. S.; Towns-Andrews, E. *Macromolecules* **1996**, *29*, 8835.
(33) Hamley, I. W.; Fairclough, J. P. A.; Ryan, A. J.; Bates, F. S.; Towns-Andrews, E. *Polymer* **1996**, *37*, 4425.
(34) Howard, P. R.; Crist, B. *J. Polym. Sci., B: Polym. Phys.* **1989**, *27*, 2269.
(35) Stack, G. M.; Mandelkern, L.; Voigt-Martin, I. G. *Macromolecules* **1984**, *17*, 321.
(36) Voigt-Martin, I. G.; Mandelkern, L. *J. Polym. Sci.: Polym. Phys. Ed.* **1984**, *22*, 1901.
(37) Leibler, L. *Macromolecules* **1980**, *13*, 1602.
(38) Sakamoto, N.; Hashimoto, T. *Macromolecules* **1995**, *28*, 6825.
(39) Helfand, E.; Wasserman, Z. R. *Macromolecules* **1976**, *9*, 879.
(40) Helfand, E.; Wasserman, Z. R. *Macromolecules* **1978**, *11*, 960.
(41) Helfand, E.; Wasserman, Z. R. *Macromolecules* **1980**, *13*, 994.
(42) Graessley, W. W.; Krishnamoorti, R.; Reichart, G. C.; Balsara, N. P.; Fetters, L. J.; Lohse, D. J. *Macromolecules* **1995**, *28*, 1260.
(43) Quiram, D. J.; Register, R. A.; Marchand, G. R.; Ryan, A. J. Manuscript submitted to *Macromolecules*.
(44) Takayanagi, M.; Yoshino, M.; Minami, S. *J. Polym. Sci.* **1962**, *61*, S7.
(45) Brandrup, J., Immergut, E. H., Eds. *Polymer Handbook*, 3rd ed.; Wiley: New York, 1989; Vol. 19.
(46) Rangarajan, P.; Haisch, C. F.; Register, R. A.; Adamson, D. H.; Fetters, L. J. *Macromolecules* **1997**, *30*, 494.

MA961524F